ORIGINAL PAPER

NONLINEAR ANALYSIS OF LEVENBERG-MARQUARDT OPTIMIZED MAGNETOHYDRODYNAMIC NANOFLUID FLOW WITH BROWNIAN AND THERMOPHORESIS EFFECTS

AAMRA UROOJ[1], HUMA TAYYAB[1], QAZI MAHMOOD UL HASSAN[1]

Manuscript received: 08.10.2025; Accepted paper: 20.11.2025;
Published online: 30.12.2025.

Abstract. *Artificial neural networks (ANNs) have transformed fluid dynamics modeling, enabling the analysis of complex phenomena with remarkable accuracy. This paper uses an ANN with the Levenberg-Marquardt optimization technique to investigate the interaction of thermophoresis diffusion and Brownian motion effects on Magnetohydrodynamic Reiner-Philippoff nanofluid flow (MHD-RPN) adjacent to a shrinking sheet. Numerical solutions are obtained by using the NDSolve solver within Mathematica, resulting in a dataset that encompasses several scenarios via parameter modifications. This data set, which contains input-output pairs, is used to train the NNs. The efficiency of the suggested ANN methodology is shown by performance assessments using MSE, error histograms, correlation, and regression plots. Graphs of temperature and concentration profiles are shown for several MHD-RPN scenarios by variations of the parameters, i.e., the thermophoresis parameter (Nt), Brownian Motion Parameter (Nb), Prandtl Number (Pr), the Schmidt number (Sc), and the thermal radiation (R), respectively. Increasing Nb increases temperature but decreases concentration, while increasing Nt improves heat and mass transport. However, radiation and greater Prandtl numbers reduce temperature and concentration. The model's effectiveness is evaluated through MSE, observed between 10^{-09} and 10^{-11} across different scenarios, confirming the robustness and efficiency of the AI-driven solution.*

Keywords: *Magnetohydrodynamic Reiner–Philippoff non-Newtonian nanofluid; shrinking sheet; thermophoresis parameter; Brownian parameter; Levenberg-Marquardt back-propagation.*

1. INTRODUCTION

Rapid heat transfer has been a growing technical discipline for decades. Researchers are employed to improve thermal conductivity and heat transfer rate. They are also attempting to decrease pumping power, frictional loss, and pressure drop for the heat transfer fluid. Nanofluid is a novel type of heat transfer fluid that has been designed to give superior thermal characteristics for heat transfer. Nanofluid is created by dissolving a small amount of nanoparticles in base fluids such as water, glycol, and others. It is worth noting that Buongiorno [1] explored convective transport in a nanofluid to better understand the observed heat transfer improvement under convective conditions. Buongiorno presented a novel model based on basic fluid and nanoparticle relative velocities. He contended that in the deficiency of turbulent effects, Brownian diffusion [2] and thermophoresis prevail. He created conservation equations based on these two effects. Many scientists who wanted to consider

[1] University of Wah, Department of Mathematics, 47040 Punjab, Pakistan. E-mail: aamraurooj321@gmail.com; humaq807@gmail.com; qazimahmood@uow.edu.pk.

https://doi.org/10.46939/J.Sci.Arts-25.4-c01

using nanofluid in conjunction with different non-Newtonian fluids turned to this discovery as their primary source of information. To mention a few, Saleem et al. [3], Waqas et al. [4] and Mahat et al. [5] researched the electrically conducting nanofluid. The Reiner-Philippoff fluid model has attracted attention recently because it can behave like a Newtonian fluid. Using the Karman-Pohlhausen approach, Kapur and Gupta [6] examined the boundary layer equations for Reiner-Philippoff fluid inside a channel. In the meantime, Reiner-Philippoff, Ellis, Ostwald de Waele, generalized Bingham, and Prandtl Eyring fluid velocity profiles were compared by Cavatorta and Tonini [7].

Applications in industry and technology require efficient, seamless work to achieve the best performance. Pure (Newtonian) water is typically used as the cooling agent. Due to their effectiveness and applicability, the usage of non-Newtonian fluids seems more and more applicable in various operations [8]. Non-Newtonian fluids come in a wide variety of varieties, each with unique properties. Shear-thickening fluids exhibit viscosity increases proportionate to shear rate, whereas shear-reducing fluids exhibit Newtonian fluid behaviour at extremely high shear rates. The Reiner-Philippoff model, one of the non-Newtonian class of models, is more fascinating to study because it depicts the behavior of a Newtonian fluid [9] at zero or large values of shear stress causes non-Newtonian behavior and affects other values. The study of the RP model has attracted the attention of many academics due to its significant role in engineering applications.

The study looked at the analysis of flows traveling over various geometries and their various effects on the flow field [10]. Since its existence affects the pace of heat transfer, including thermal radiation in the flow presents greater difficulties and substantial contributions. Thermal radiation is useful in solar technologies [11], aircraft, medicine, and spacecraft operations. Rosseland invented thermal radiation, and Ghosh, Mukhopadhyay, Yashkun, and others have greatly expanded on his concepts [12], Agbaje et al. [13, 14], and Muhammad et al. [15] fluid flow in MHD non-Newtonian, including fluids with nanoparticles over a shrinking sheet, was investigated. Due to its capacity to affect fluid characteristics, the influence of the magnetic field, also known as magnetohydrodynamics (MHD), is one of the frequently taken into consideration effects in fluid flow investigations. The drag Lorentz force is launched when MHD is present, which might prevent boundary layer separation. In a study by Rashidi et al. [16], the analysis of the MHD's presence was emphasized. In addition, Hussain et al. [17] and Sheikholeslami et al. carried out a study on MHD flow in the free convection mode. Haq et al. [18], on the other hand, explored the MHD flow by incorporating the nanoparticles. Khan et al. [19, 20], Srinivasulu and Goud [21], Khashi'ie et al. [22], Zhang et al. [23], all reported on further work on MHD flow. Additionally, Ashwinkumar et al. [24] have reported on their investigation into MHD hybrid nanofluid flow over various geometries. The research of the RPF model combined with nanofluid is innovative; however, it is constrained and leaves several gaps that need to be filled. Therefore, the goal of this study is to deepen our understanding of the unique properties of the Reiner-Philippoff fluid embedded in thermophoresis and Brownian diffusion under MHD conditions.

With recent technology innovations, more contemporary and efficient controllers for complicated processes are being built. The Artificial Neural Network (ANN) [25, 26] has emerged as a viable alternative to the automatic control of nonlinear systems with many inputs and outputs. These systems have proven their capacity to address a wide range of operations, from simple applications to sophisticated industrial processes. To represent varied applications in expanded sectors, a stochastic numerical computing solver was constructed using the capabilities of evolutionary/swarming computing-based optimization methodologies related to linear and nonlinear differentiation and neural network models for solving equations [27,28]. Contemporary stochastic numerical computer solver implementations include nonlinear circuits [29], atomic physics, thermodynamics, astrophysics,

magnetohydrodynamics [30], haemoglobin, fluid dynamics [31], nanotechnology [32], and random matrix models [33, 34]. All of the facts established the significance of synthetic solutions based on intelligent algorithms (AI) developed research domain and studied the latest algorithms for non-linear fluid can be helpful for finer analysis of complex dynamic problems [35].

The objective of this research is to implement an ANN [36] model to analyze the effect of MHD-RPN between shrinking sheets. To train, validate, and assess performance valuation indicators, we used three multi-layer feed-forward networks using the back-propagation LMM algorithmic program [31, 34, 37]. The ANN approach is a way of processing data that is based on simulating the human brain. Models for forecasting and evaluating are regularly made using it. Layers of several mutually interconnected neurons make up an ANN. An ANN normally consists of three different sorts of layers: input, hidden, and output. Outside sources provide information about the enquiry to the input layer. The hidden layer(s) connect to other levels rather than the outside world. The result is sent outside by the output layer. Each input neuron in the feed-forward ANN has a weight coefficient. These weight coefficients are multiplied by the input signals to determine each neuron's input signal, which is subsequently added. The network architecture is defined as the number of hidden layers and hidden neurons. The input volume and network architecture are closely connected. If the performance of the first layer is poor, it is recommended to start with one hidden layer and work your way up to two hidden layers. The number of neurons in the hidden layer will boost the network's power.

It has not yet been investigated how the MHD-RPN model uses an ANN model. Since Brownian and thermophoresis parameter effects were taken into account, the originality of the current work focused on the usefulness of the ANN approach. According to the results of the ANN process, several parameters are investigated, and numerical results are provided. No prior studies of this nature have been carried out, according to a thorough review of the literature. Because it attempts to fill a vacuum in the corpus of knowledge in this field, this study is significant. The results are presented and developed using graphs and numerical benchmarks. Section 2 presents the mathematical model for the issue under investigation. In section 3, the LMM approach is laid out. The effects of different factors on physical quantities are covered in Section 4. Section 5 concludes.

2. MATHEMATICAL FORMULATION

The steady two-dimensional boundary layer flow of a Reiner-Philippoff nanofluid across a declining surface is taken into account; it is assumed that the external pressure on the plate is in the x-direction and that the base fluids contain nanoparticles. $U_w(x) = ax^{\frac{1}{3}}$ represents velocity with $a > 0$. The magnetic field $B(x) = B_0 x^{-\frac{1}{3}}$, where B_0 is the constant magnetic strength. The radiative heat flux will be considered as $q_r = -\left(\frac{4\,\sigma^*}{3k^*}\right)\left(\frac{\partial T^4}{\partial y}\right)$ and $T^4 \cong 4T_\infty^3 T - 3T_\infty^4$. Here k^* and σ^* represent the Stefan-Boltzmann constants and the mean absorption, respectively. Brownian and thermophoresis diffusion D_B & D_T effects are engaged. The model used to illustrate the current issue underwent boundary layer approximations first. Flow geometry for the thermophoresis diffusion and Brownian motion effects on magnetohydrodynamic Reiner-Philippoff nanofluid flow adjacent to a shrinking sheet is presented via Fig. 1, whereas Fig. 2 is constructed for the neural networks diagram.

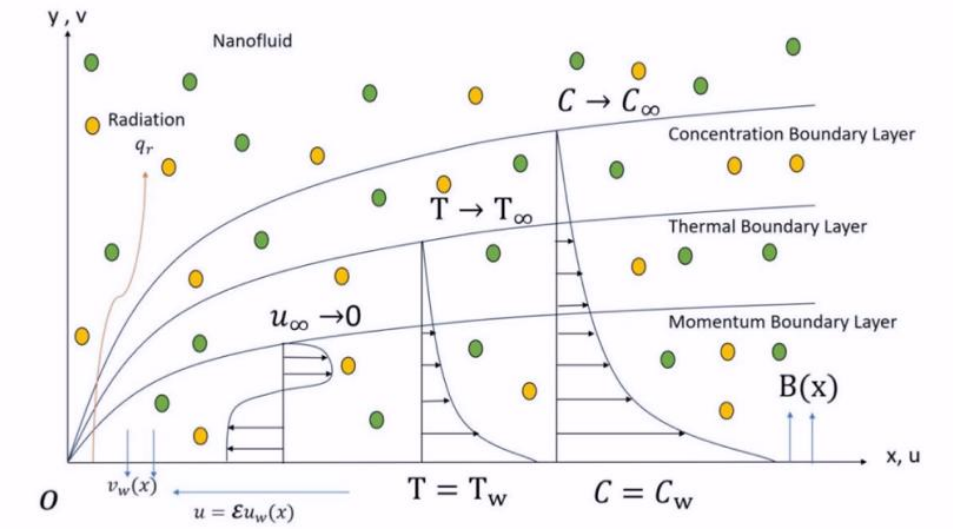

Figure 1. Flow of Geometry.

The controlling boundary layer equations are hence [38, 39]

$$\frac{\partial u}{\partial x} + \frac{\partial \mathrm{v}}{\partial y} = 0\,, \tag{1}$$

$$\frac{\partial u}{\partial y} = \frac{\tau}{\mu_\infty + \frac{\mu_0 - \mu_\infty}{1+\left(\frac{\tau}{\tau_S}\right)^2}}\,, \tag{2}$$

$$u\frac{\partial u}{\partial x} + v\frac{\partial u}{\partial y} = \frac{1}{\rho}\frac{\partial \tau}{\partial y} - \frac{\sigma}{\rho}B^2 u\,, \tag{3}$$

$$u\frac{\partial T}{\partial x} + v\frac{\partial T}{\partial y} = \left(\frac{k}{\rho C_p} + \frac{16\sigma^* T_\infty^3}{3(\rho C_p)k^*}\right)\frac{\partial^2 T}{\partial y^2} + \delta\left(D_B\frac{\partial C}{\partial y}\frac{\partial T}{\partial y} + \frac{D_T}{T_\infty}\left(\frac{\partial T}{\partial y}\right)^2\right), \tag{4}$$

$$u\frac{\partial C}{\partial x} + v\frac{\partial C}{\partial y} = D_B\frac{\partial^2 C}{\partial y^2} + \frac{D_T}{T_\infty}\frac{\partial^2 T}{\partial y^2}\,. \tag{5}$$

as originally viewed by subjected to the following boundary condition:

$$\begin{gathered} u = \varepsilon u_w(x),\ v = v_w(x),\ T = T_w,\ C = C_w \text{ at } y = 0; \\ u \to 0,\ T \to T_\infty,\ C \to C_\infty \text{ as } y \to \infty. \end{gathered} \tag{6}$$

Here, we take constant values T_w , C_w While the ambient temperature T_∞ and nanoparticle fraction C_∞ have reached their maximum levels and are infinitesimally small.

2.1. SIMILARITY TRANSFORMATION

Study the similarity variables [40, 41]:

$$\begin{gathered} \psi = \sqrt{av}x^{2/3}f(\eta),\ \tau = \rho\sqrt{a^3 v}g(\eta), \theta(\eta) = \frac{T - T_\infty}{T_w - T_\infty}, \chi(\eta) = \frac{C - C_\infty}{C_w - C_\infty},\ \eta \\ = \frac{y}{x^{1/3}}\sqrt{\frac{a}{v}}\,, \end{gathered} \tag{7}$$

with the stream function ψ. Here:

$$u = \frac{\partial \psi}{\partial y} = ax^{1/3} f'(\eta),\ v = -\frac{\partial \psi}{\partial x} = -\sqrt{av}x^{-1/3}\left(\frac{2}{3}f(\eta) - \frac{1}{3}\eta f'(\eta)\right), \tag{8}$$

$$v_w(x) = -\frac{2}{3}\sqrt{av}x^{-1/3}. \tag{9}$$

with $v = \mu_\infty/\rho$, In the meantime, the constant mass flux parameter is represented by $f(0) = S$. Here, $S = 0$ and $S > 0$ Indicate the suction and impermeable instances. Then, one succeeds:

$$g = f''\left(\frac{\lambda\gamma^2 + g^2}{\gamma^2 + g^2}\right), \tag{10}$$

$$g' + \frac{2}{3}ff'' - \frac{1}{3}f^2 - Mf' = 0, \tag{11}$$

$$\frac{1}{\Pr}\left(1 + \frac{4}{3}R\right)\theta'' + \frac{2}{3}f\theta' + Nb\chi'\theta' + Nt\theta'^2 = 0, \tag{12}$$

$$\chi'' + Scf\chi' + \frac{Nt}{Nb}\theta'' = 0, \tag{13}$$

$$\theta(0) = 1, f(0) = S,\ \chi(0) = 1,\ f'(0) = \varepsilon; f'(\eta) \to 0,\ \theta(\eta) \to 0,\ \chi(\eta) \to 0 \text{ as } \eta \to \infty. \tag{14}$$

where $\varepsilon < 0$ shows a shrinking sheet.

$$\Pr = \frac{\mu C_p}{k}, Sc = \frac{v}{D_B}, M = \frac{\sigma}{\rho a}B_0^2,\ \lambda = \frac{\mu_0}{\mu_\infty},\ R = \frac{4\sigma^* T_\infty^3}{kk^*}, \gamma = \frac{\tau_s}{\rho\sqrt{a^3 v}},$$
$$Nb = \frac{\delta D_B(C_w - C_\infty)}{v}, Nt = \frac{\delta D_T(T_w - T_\infty)}{vT_\infty}. \tag{15}$$

2.2. METHODOLOGY

The method approximates the inherently non-linear nature of the MHD-RPN system by initially reducing the governing partial differential equations (PDEs) to obtain a set of ordinary differential equations (ODEs) by using a similarity transformation. An advanced Adams numerical method is employed for generating the dataset required in the ANN-LMA for training the neural networks. 'NDSolve' in Wolfram Mathematica is used to solve equations of MHD-RPN using the Adam numerical solver. Then we shift the result from Mathematica to MATLAB and select input from 0 to 20 with a step size of 100. The 'nftool' algorithm, which is a useful tool in the MATLAB software package's neural networks (NN) toolbox, is used to carry out the methodology described here for the suggested back-propagated NN, and the Levenberg-Marquardt approach is used to determine the network weights. The approach is divided into two sections: the first section contains the key information needed to create a dataset for LM-NN, and the second section describes the steps

taken to put that information into practice. This design of the neural network is the basis for the configuration in Figs. 2a and 2b represent the overall flow chart of MHD-RPN. Since they introduce non-linearity in the output of individual neurons, activation functions form a crucial part of this architecture. Since it allows the network to view and comprehend complicated patterns and relationships in the data, this non-linearity is necessary. In addition, by enabling gradient-based weight and bias adjustments during training, activation functions assist the back-propagation method. As a result, the method enhances the precision and stability of flow measurements, particularly when non-Newtonian fluids are concerned or non-invasive assessments of drilling fluids are being performed.

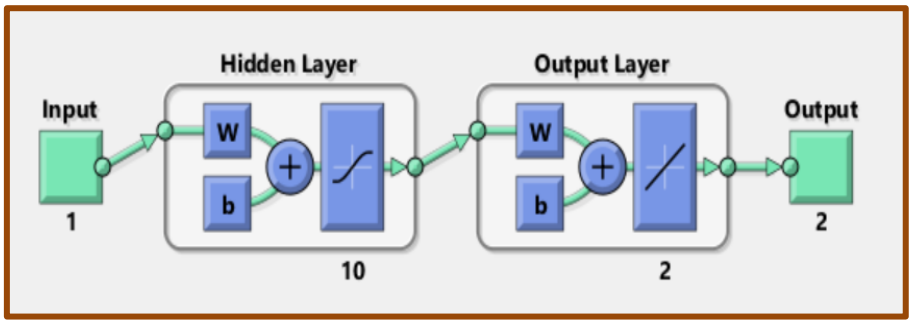

a

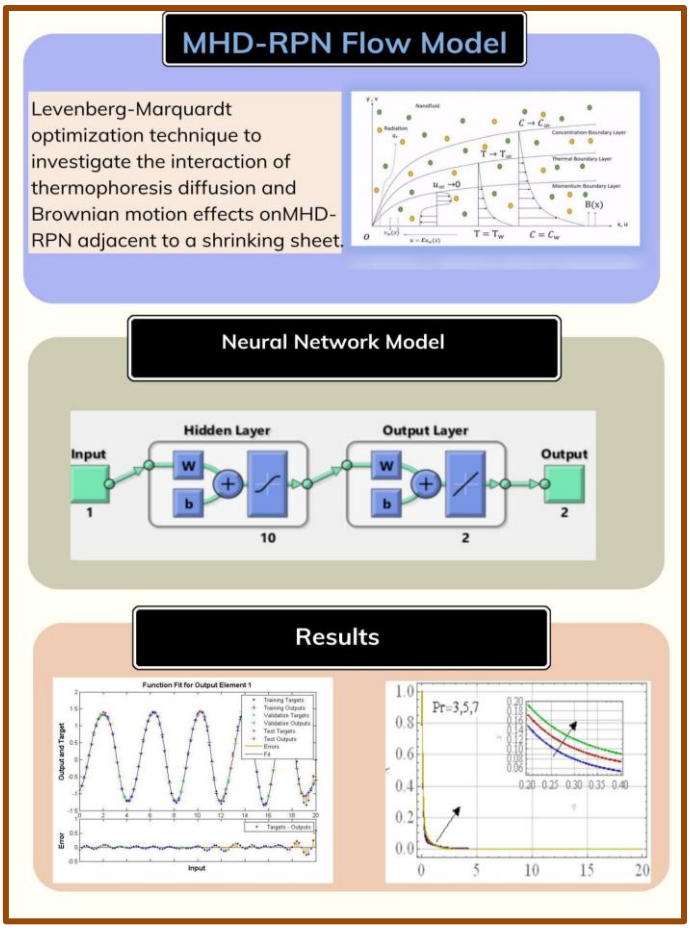

b

Figure 2. a. Neural Network for MHD-RPN; b. Flow Chart of MHD-RPN.

Table 1. Constant parameter values

Nt	Nb	Pr	R	Sc	M	S	γ	λ	ϵ
0.1	0.1	7	5	5	0.01	2.4	0.1	1.5	-1

3. RESULTS AND DISCUSSION

3.1. ANN MODEL RESULTS

The NDSolve solver is used to create the reference data set in the Mathematica program. Diagrams are used to graphically illustrate the numerical solutions that occur. Table 2 displays five scenarios with three cases for each scenario. For all NDSolve method scenarios, the step size is 0.20, and the input range is 0 to 20. After creating the data set, the RPN model is solved using the "nftool" command. Figs. 3-7 show the MHD-RPN solution for each scenario of Case 1 in the form of a performance plot, histogram plot, regression plot, and training state and fitting plot. Figs. 3-7 show the plots of the Performance plot, Error histogram, Regression, Training state, and. A regression plot is a statistical graph that depicts the correlation between two variables.

Table 2. Variations of physical quantities of MHD-RPN.

Scenarios	Cases	Physical Quantities				
		Nt	Nb	Pr	Sc	R
01	1	0.1	0.1	7	5	5
	2	0.3	0.1	7	5	5
	3	0.5	0.1	7	5	5
02	1	0.1	0.1	7	5	5
	2	0.1	0.3	7	5	5
	3	0.1	0.5	7	5	5
03	1	0.1	0.1	3	5	5
	2	0.1	0.1	5	5	5
	3	0.1	0.1	7	5	5
04	1	0.1	0.1	7	1	5
	2	0.1	0.1	7	3	5
	3	0.1	0.1	7	5	5
05	1	0.1	0.1	7	5	5
	2	0.1	0.1	7	5	10
	3	0.1	0.1	7	5	15

Fig. 3 shows the mean-squared error curves for training, testing, and validation of case 1 for all possible scenarios. The figure makes it clear that the best validation performance for Case 1 of Scenario 1 is 7.55×10^{-11}, Scenario 2, the best validation performance is 3.52×10^{-9}, Scenario 3, the best validation performance is 7.47×10^{-11}, Scenario 4, the best validation performance is 7.87×10^{-11}, Scenario 5, the best validation performance is 1.03×10^{-10} in time less than 5 sec in all. In a performance plot, the target variable's actual values are shown on the horizontal axis, and the MHD-RPN model's predicted values are shown on the vertical axis. The error histogram for case 1 across all five scenarios is displayed in Fig. 4. The maximum values depicting the errors are roughly equal to zero, as can be seen from the plots of the error histograms, which supports the validity of the method. The training state analysis for Case 1 for all MHD-RPN scenarios is depicted graphically in Fig. 5. A balance of gradient and mu values suggests that the neural network is making weight updates in a controlled and efficient manner.

The criteria for training are 80%, validation is 10% and testing is 10%. Table 3 below shows statistical results that are obtained after training the model on a given data set.

Table 3. Performance of MHD-RPN.

Scenarios	Case	MSE data		Performance	Gradient	Mu	Final Epoch	Time
		Training	Testing					
1	1	3.43×10^{-10}	2.31×10^{-10}	7.55×10^{-11}	9.9×10^{-8}	$1.00\times10^{-0.8}$	310	04s
	2	3.96×10^{-10}	8.40×10^{-10}	7.21×10^{-10}	9.9×10^{-8}	$1.00\times10^{-0.8}$	15	<5s
	3	3.38×10^{-10}	3.55×10^{-11}	3.52×10^{-9}	9.9×10^{-8}	$1.00\times10^{-0.8}$	14	<5s
2	1	3.67×10^{-11}	1.47×10^{-10}	3.52×10^{-9}	9.9×10^{-8}	$1.00\times10^{-0.8}$	31	<5s
	2	7.68×10^{-10}	1.27×10^{-11}	9.99×10^{-11}	9.9×10^{-8}	$1.00\times10^{-0.8}$	388	4s
	3	2.22×10^{-11}	3.13×10^{-10}	4.73×10^{-10}	9.9×10^{-8}	$1.00\times10^{-0.8}$	91	<5s
3	1	1.40×10^{-11}	1.17×10^{-10}	7.47×10^{-11}	9.9×10^{-8}	$1.00\times10^{-0.8}$	268	03s
	2	2.44×10^{-10}	1.92×10^{-11}	4.87×10^{-9}	9.9×10^{-8}	$1.00\times10^{-0.8}$	69	01s
	3	4.08×10^{-10}	4.375×10^{-9}	6.99×10^{-11}	9.9×10^{-8}	$1.00\times10^{-0.8}$	17	<5s
4	1	3.20×10^{-10}	2.40×10^{-10}	7.87×10^{-11}	9.9×10^{-8}	$1.00\times10^{-0.8}$	317	04s
	2	1.62×10^{-11}	2.20×10^{-10}	2.11×10^{-10}	9.9×10^{-8}	$1.00\times10^{-0.8}$	64	<5s
	3	4.09×10^{-10}	4.55×10^{-11}	2.99×10^{-11}	9.9×10^{-8}	$1.00\times10^{-0.8}$	17	<5s
5	1	3.90×10^{-11}	7.05×10^{-10}	1.03×10^{-10}	9.9×10^{-8}	$1.00\times10^{-0.8}$	18	<5s
	2	3.31×10^{-10}	1.70×10^{-11}	2.99×10^{-11}	9.9×10^{-8}	$1.00\times10^{-0.8}$	34	<5s
	3	3.24×10^{-10}	4.17×10^{-11}	2.99×10^{-9}	9.9×10^{-8}	$1.00\times10^{-0.8}$	74	<5s

The regression analysis for Case 1 for all MHD-RPN scenarios is depicted graphically in Fig. 6. According to the regression graphs, the MHD-RPN achieved the best results across all scenarios for the many criteria mentioned. A higher R-squared value in a regression plot denotes that the data points are nearer the regression line and that the regression line adequately fits the data. This indicates that the model does a better job of describing how the independent and dependent variables relate to one another. Fig. 7 shows the fitness curve for all scenarios in Case 1. The fitness curve analysis shows that there is no noise and that the trends for the actual and projected values are the same, proving that the data prediction model is efficient.

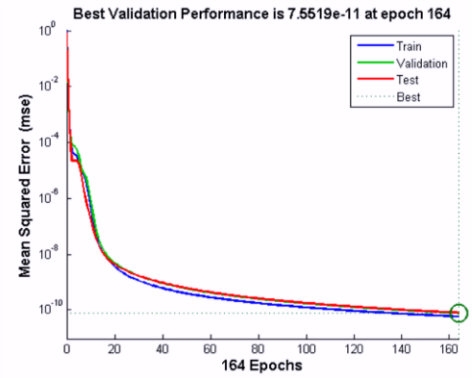

Performance plot for Scenario 1

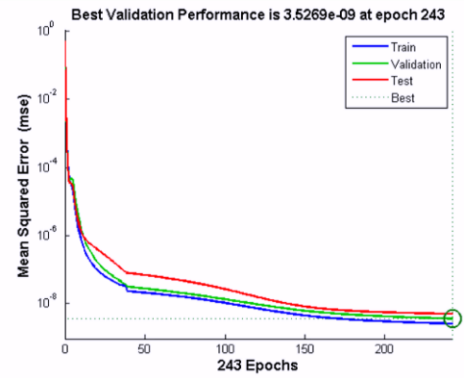

Performance plot for Scenario 2

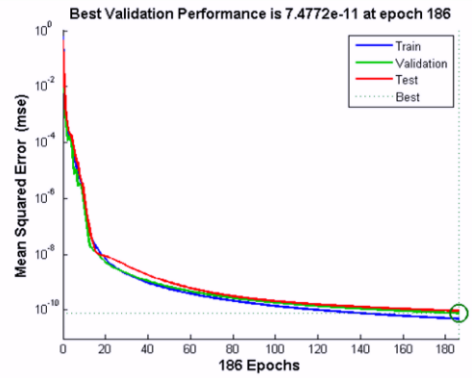

Performance plot for Scenario 3

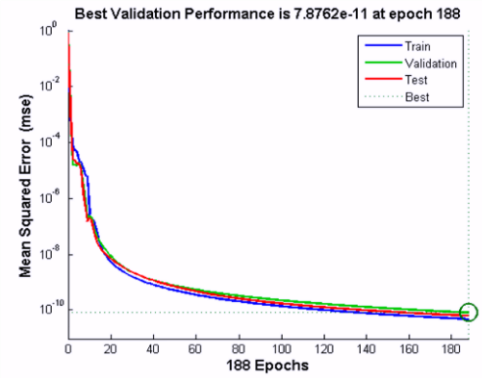

Performance plot for Scenario 4

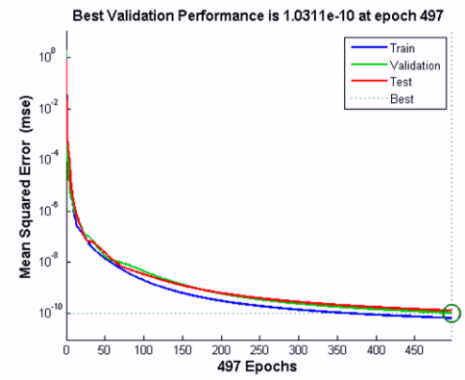

Performance plot for Scenario 5

Figure 3. Performance or MSE plots for MHD-RPN

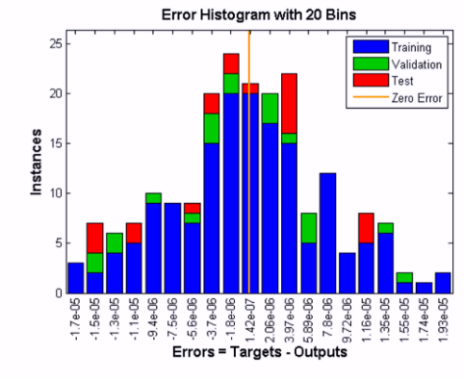

Fitness plot for Scenario 1

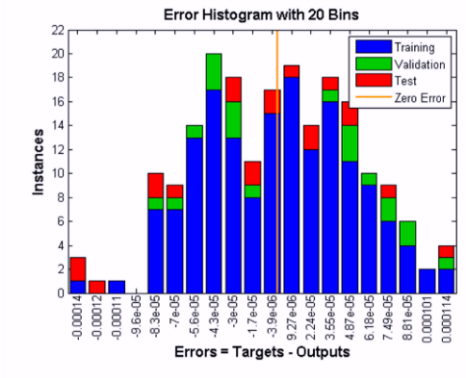

Fitness plot for Scenario 2

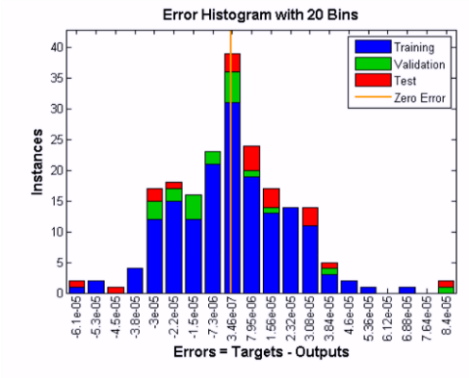

Fitness plot for Scenario 3

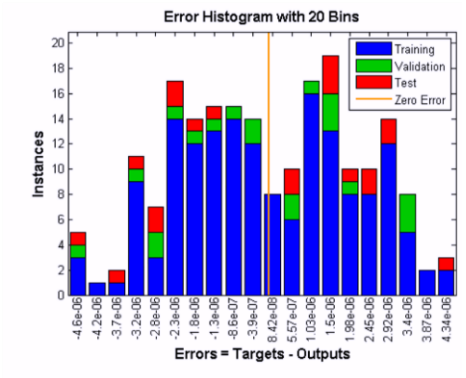

Fitness plot for Scenario 4

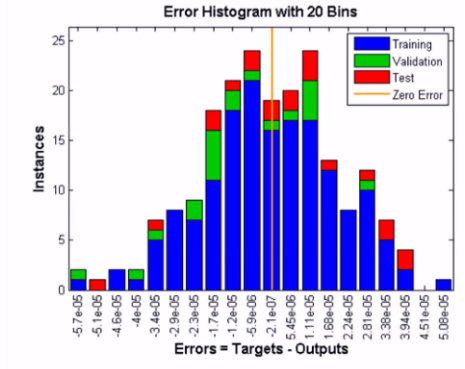

Fitness plot for Scenario 5

Figure 4. Error histogram for MHD-RPN.

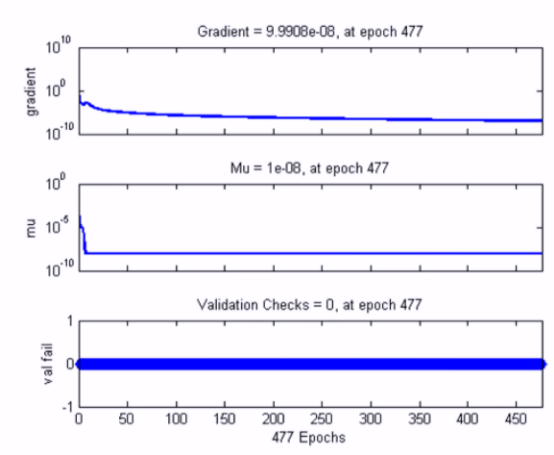

Fitness plot for Scenario 1

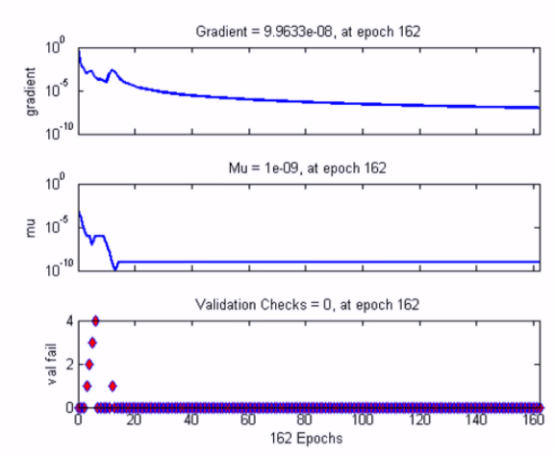

Fitness plot for Scenario 2

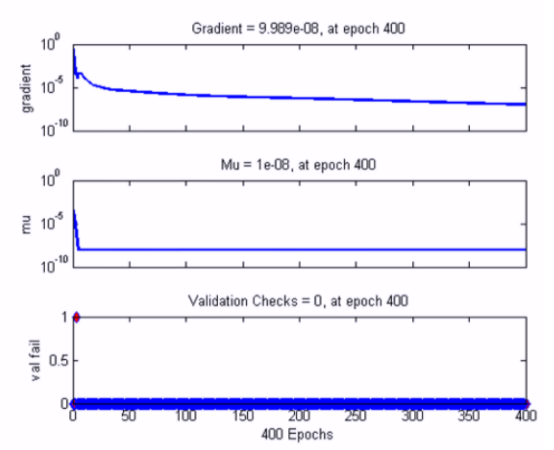

Fitness plot for Scenario 3

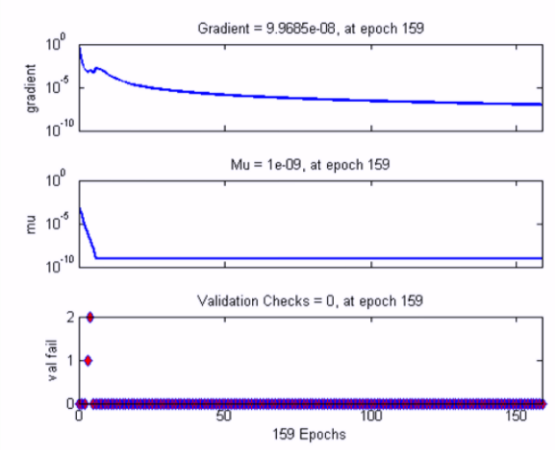

Fitness plot for Scenario 4

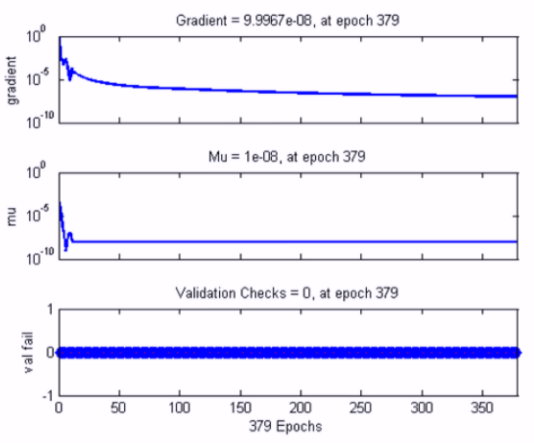

Training state plot for Scenario 5

Figure 5. Training state Plot for MHD-RPN

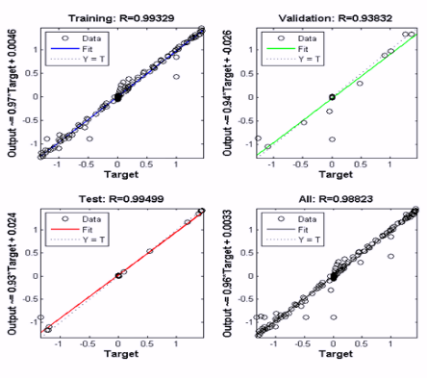

Regression Plot for Scenario 1

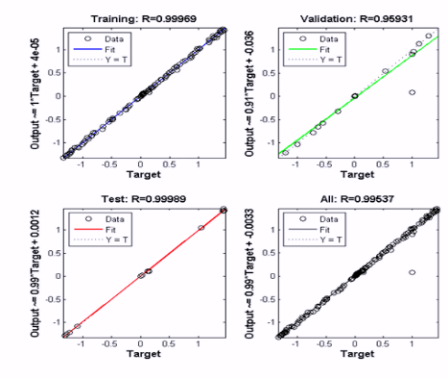

Regression Plot for Scenario 2

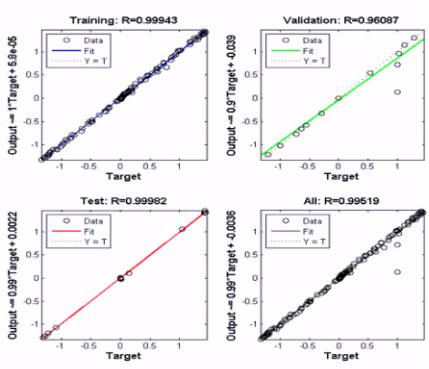

Regression Plot for Scenario 3

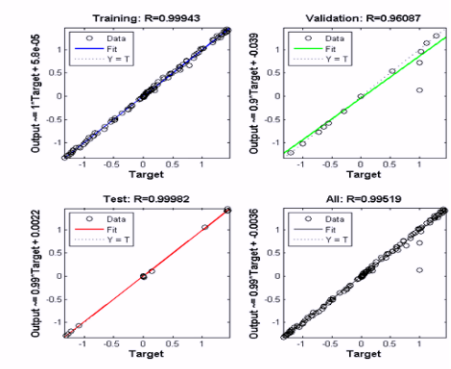

Regression Plot for Scenario 4

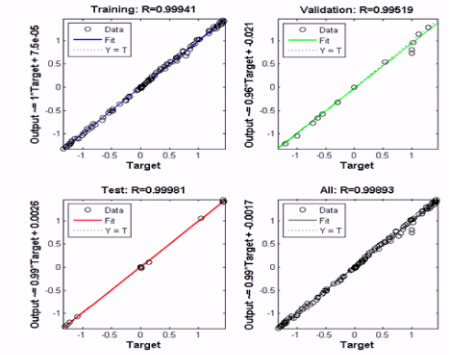

Regression Plot for Scenario 5

Figure 6. Regression Plot for MHD-RPN

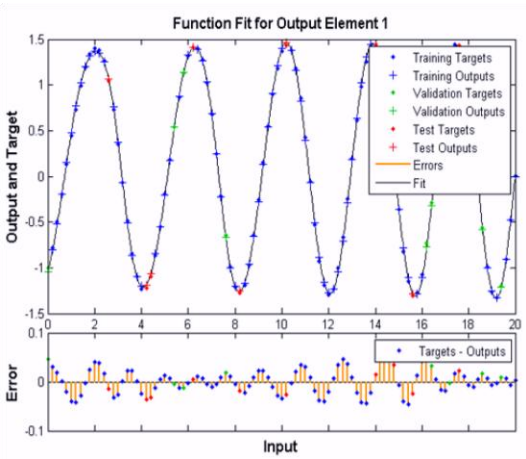

Fitness plot for Scenario 1

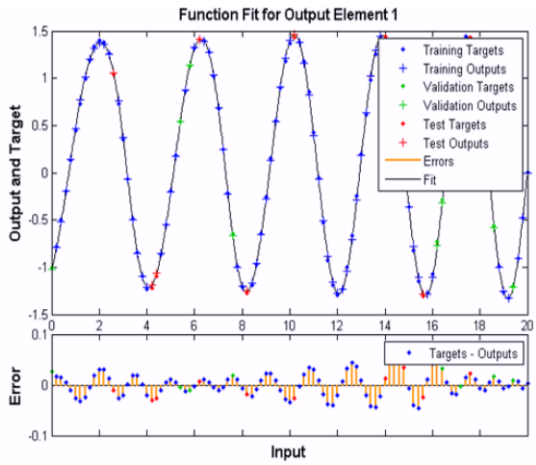

Fitness plot for Scenario 2

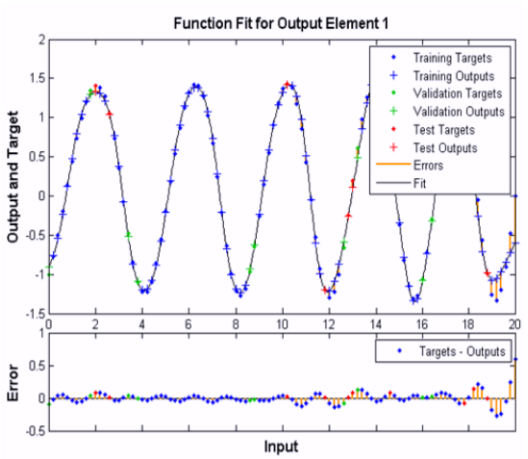

Fitness plot for Scenario 3

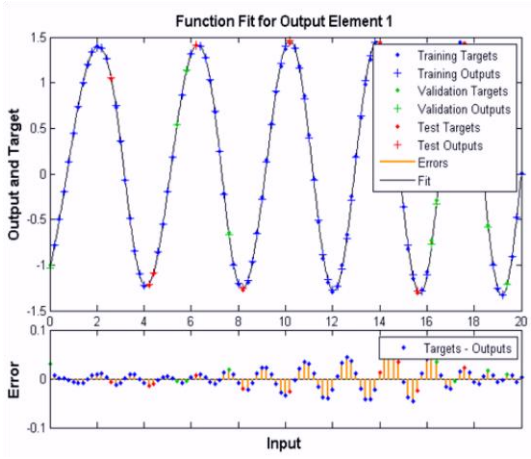

Fitness plot for Scenario 4

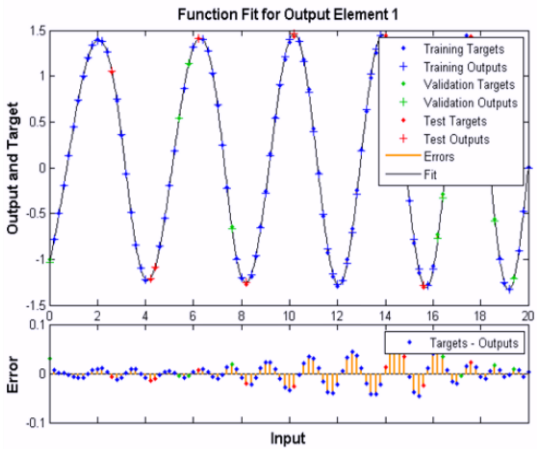

Fitness plot for Scenario 5

Figure 7. Fitting plot for MHD-RPN

3.2. DISCUSSION ON THE TEMPERATURE AND CONCENTRATION PROFILES

Figs. 8 and 9 show how Nb and Nt have an impact on temperature and concentration profiles. Although the concentration boundary layer thins with increases in Nb shown in Fig. 8a, the thermal boundary layer thickens with an increase in Nb shown in Figure 8b. These findings suggest that the speed of mass transfer intensity tends to grow as Nb rises while decreasing the heat transfer rate. However, Nt has the effect of increasing both the thermal addition to the concentration boundary layers, as shown in Fig. 9 (a and b), which increases heat transfer and mass transfer rates.

Figs. 8 and 9 are also included so that you can see how Nb and Nt affect the rates of mass and heat transmission. From a purely physical perspective, the Brownian motion causes the fluid particles to collide. As a result, the nanoparticles in suspension produce more kinetic energy when Nb rises, which raise the fluid's temperature and, in turn, create the thermophoresis force. Higher values of Nt thereby increasing fluid temperature and enhancing the fluid's concentration as a result.

In Fig. 10, it is discussed how the thermal radiation parameter R affects the Temperature $\theta(\eta)$ and Concentration $\chi(\eta)$ profiles. Physically, the presence of thermal radiation causes the radiative heat flux to rise relative to the functional flow. The thickness of the boundary layer expands as a result of inclusion in R, increasing the temperature

distribution in the flow zone of R as the flow strength increases. Since a larger R is associated with greater temperature, this results in a thinner boundary layer, which reduces the fluid concentration near the surface. As shown in Fig. 11, the temperature profile decreases as the Prandtl number rises, whereas the concentration profile increases as the Prandtl number increases.

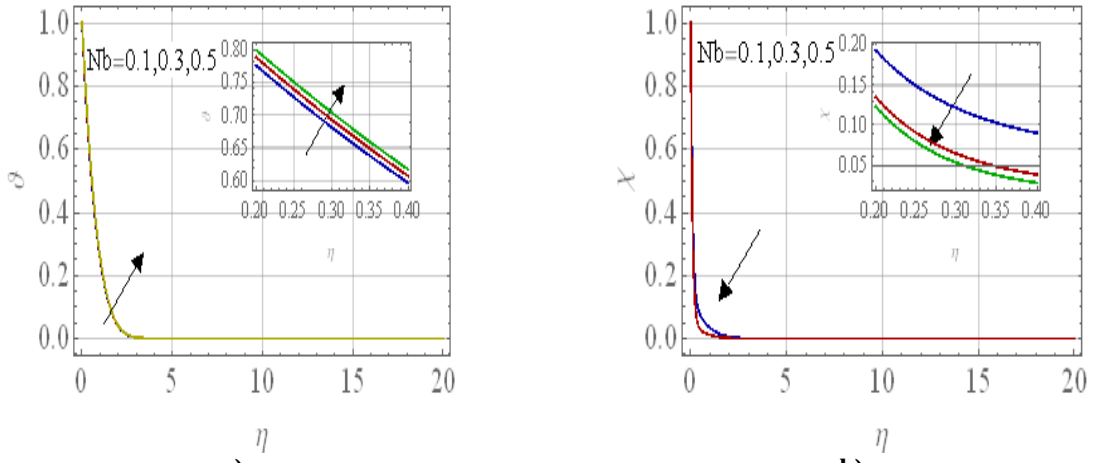

a) **b)**

Figure 8. a) $\theta(\eta)$; b) $\chi(\eta)$ profiles against Nb.

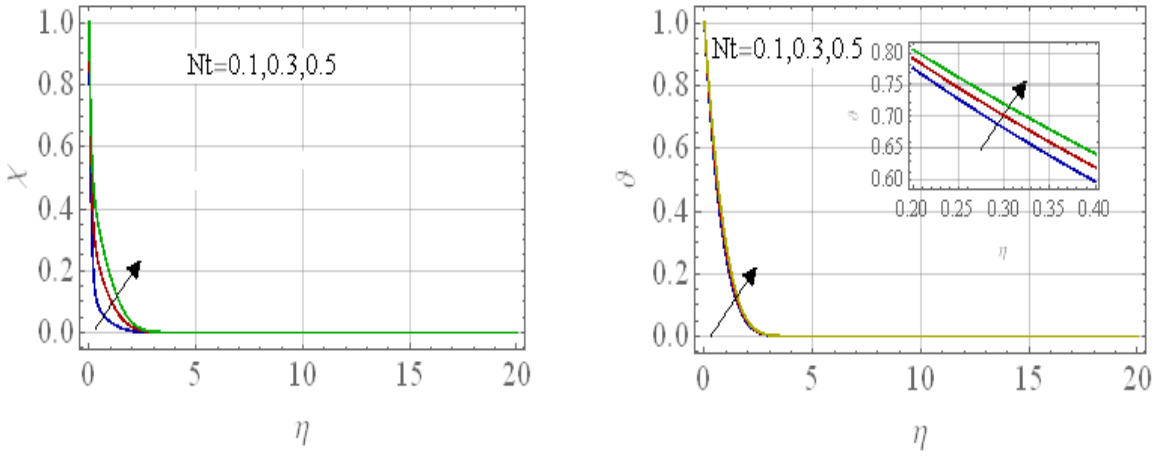

a) **b)**

Figure 9. a) $\theta(\eta)$; b) $\chi(\eta)$ profiles againt Nt.

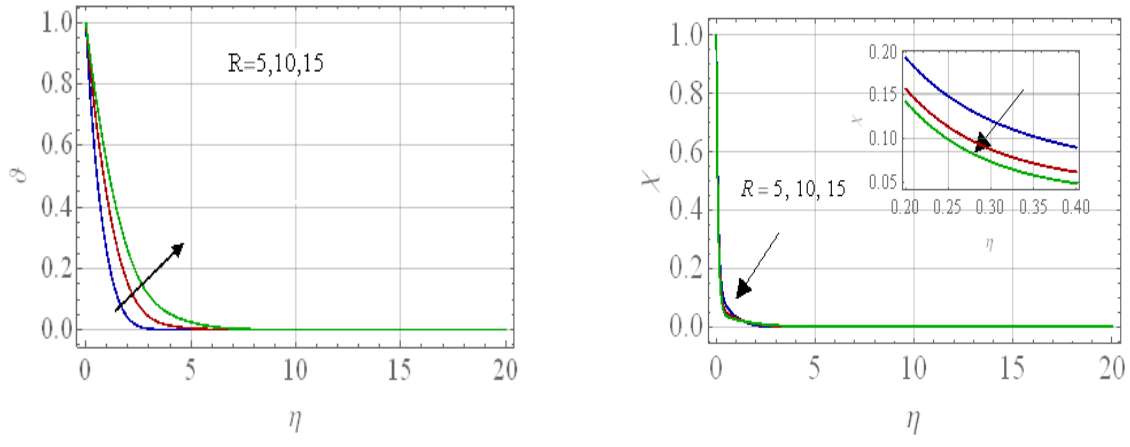

a) **b)**

Figure 10. a) $\theta(\eta)$; b) $\chi(\eta)$ profiles against R.

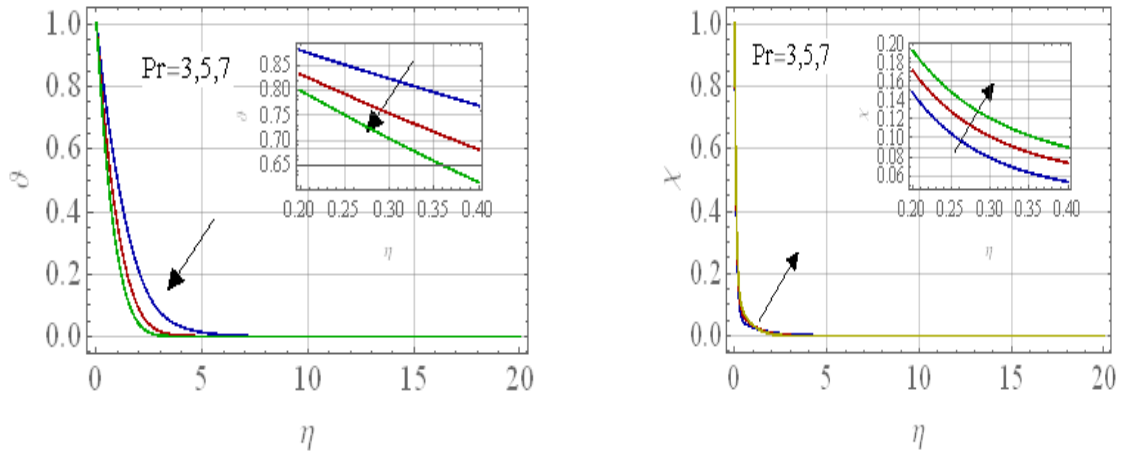

a) **b)**

Figure 11. a) $\theta(\eta$; b) $\chi(\eta)$ profiles against Pr

4. CONCLUSIONS

This paper uses an ANN with the Levenberg-Marquardt optimization technique to investigate the interaction of thermophoresis diffusion and Brownian motion effects on MHD-RPN flow adjacent to a shrinking sheet. The plots show that the Levenberg-Marquardt Back-propagated prediction by MHD-RPN acceptably fits the model, and one can suitably modify the model by changing the various parameters that may improve the accuracy and efficacy of results by the aforementioned techniques.

– The performance of the ANN model is validated by error histograms that are tightly clustered within the range of 10^{-06} to 10^{-08}, centered near the zero line.

– Additionally, the model's high accuracy is confirmed by the mean square error (MSE), which falls between 10^{-09} and 10^{-12}.

– Temperature distribution is higher, whereas the Concentration decays as the Brownian motion parameter Nb is increased.

– The heat and mass transfer rates increased as the thermophoresis parameter Nt increased. But as the radiation parameter is raised, thermal and mass progress are constrained.

– Temperature distribution and concentration are higher for the thermophoresis parameter Nt.

– Concentration has maximum values for the Prandtl number and decays for the radiation parameter.

– The temperature profile decreases as the Prandtl number rises.

– The regression plots indicate that the results obtained from ANN and the Adam numerical solver are the same and compatible.

REFERENCES

[1] Buongiorno, J., ASME Journal of Heat and Mass Transfer, **128**(3), 240, 2006.

[2] Gillespie, D. T., Seitaridou, E., *Simple Brownian diffusion: an introduction to the standard thoretical models*, Oxford University Press, USA, 2013.

[3] Saleem, S., Rafiq, H., Al-Qahtani, A., El-Aziz, M. A., Malik, M., Animasaun, I., *Mathematical Problems in Engineering*, **2019**, 478037, 2019.

[4] Waqas, M., Gulzar, M. M., Dogonchi, A., Javed, M. A., Khan, W., *Applied Nanoscience*, **9**, 2031, 2019.
[5] Mahat, R., Rawi, N. A., Kasim, A. R. M., Shafie, S., *Malays. Journal of Fundamental and Applied Sciences*, **16**, 166, 2020.
[6] Kapur, J., Gupta, R., *Applied Scientific Research, Section A*, **14**, 13, 1965.
[7] Cavatorta, O. N., Tonini, R. D., *International Communications in Heat and Mass Transfer*, **14**, 359, 1987.
[8] Sabir, Z., *European Physical Journal Plus*, **137**, 638, 2022.
[9] Koyré, A., *Newtonian Studies*, Harvard University Press, 1965.
[10] Sabir, Z., Alhazmi, S. E., *Physica Scripta*, **98**, 105233, 2023.
[11] Mekhilef, S., Faramarzi, S., Saidur, R., Salam, Z., *Renewable and Sustainable Energy Reviews*, **18**, 583, 2013.
[12] Yashkun, U., Zaimi, K., Bakar, N. A. A., Ishak, A., Pop, I., *International Journal of Numerical Methods for Heat and Fluid Flow*, **31**, 1014, 2020.
[13] Shah, Z., Kumam, P., Deebani, W., *Scientific Reports*, **10**, 4402, 2020.
[14] Agbaje, T., Mondal, S., Motsa, S. S., Sibanda, P., *Alexandria Engineering Journal*, **56**, 81, 2017.
[15] Muhammad, K., Hayat, T., Alsaedi, A., *Waves in Random and Complex Media*, **34**(3), 2040, 2021.
[16] Rashidi, M., Abelman, S., Mehr, N. F., *International Journal of Heat and Mass Transfer*, **62**, 515, 2013.
[17] Sheikholeslami, M., Gorji-Bandpy, M., Ganji, D., *Journal of the Taiwan Institute of Chemical Engineers*, **45**, 1204, 2014.
[18] Haq, R. U., Rashid, I., Khan, Z., *Journal of Molecular Liquids*, **243**, 682, 2017.
[19] Khan, U., Zaib, A., Khan, I., Nisar, K. S., *Journal of Materials Research and Technology*, **9**, 188, 2020.
[20] Khan, U., Zaib, A., Khan, I., Baleanu, D., Sherif, E. S. M., *Journal of Materials Research and Technology*, **9**, 3817, 2020.
[21] Srinivasulu, T., Goud, B. S., *Case Studies in Thermal Engineering*, **23**, 100819, 2021.
[22] Khashi'ie, N. S., Arifin, N. M., Rashidi, M. M., Hafidzuddin, E. H., Wahi, N., *Journal of Thermal Analysis and Calorimetry*, **139**, 3635, 2020.
[23] Zhang, X. H., Abidi, A., Ahmed, A. E. S., Khan, M. R., El-Shorbagy, M., Shutaywi, M., *Case Studies in Thermal Engineering*, **26**, 101184, 2021.
[24] Ashwinkumar, G., Samrat, S., Sandeep, N., *International Communications in Heat and Mass Transfer*, **127**, 105563, 2021.
[25] Sabir, Z., Said, S. B., Al-Mdallal, Q., Bhat, S. A., *Expert Systems with Applications*, **238**, 122224, 2024.
[26] Sabir, Z., Said, S. B., Al-Mdallal, Q., *Intelligent Systems with Applications*, **21**, 200309, 2024.
[27] Shoaib, M., Raja, M. A. Z., Sabir, M. T., Bukhari, A. H., Alrabaiah, H., Shah, Z., *Computer Methods and Programs in Biomedicine*, **202**, 105973, 2021.
[28] AbuAli, N., Sabir, Z., *Journal of King Saud University Computer and Information Sciences*, **36**, 101890, 2024.
[29] Shoaib, M., Anwar, N., Ahmad, I., Naz, S., Kiani, A. K., Raja, M. A. Z., *Biomedical Signal Processing and Control*, **84**, 104797, 2023.
[30] Shoaib, M., Raja, M. A. Z., Khan, M. A. R., Farhat, I., Awan, S. E., *Surfaces and Interfaces*, 25, 101243, 2021.
[31] Shoaib, M., Abbasi, A. Z., Raja, M. A. Z., Nisar, K. S., *Chaos, Solitons and Fractals*, **165**, 112812, 2022.

[32] Shoaib, M., Zubair, G., Nisar, K. S., Raja, M. A. Z., Khan, M. I., Gowda, R. P., *International Communications in Heat and Mass Transfer*, **129**, 105683, 2021.
[33] Freitas, N., Delvenne, J. C., Esposito, M., *Physical Review X*, **11**, 031064, 2021.
[34] Shoaib, M., Kausar, M., Nisar, K. S., Raja, M. A. Z., *Waves in Random and Complex Media*, **1**, 1, 2022.
[35] Shoaib, M., Abukhaled, M., Kainat, S., Nisar, K. S., Raja, M. A. Z., Zubair, G., *International Journal on Recent and Innovation Trends in Computing and Communication*, **15**, 80, 2022.
[36] Maind, S. B., Wankar, P., *International Journal on Recent and Innovation Trends in Computing and Communication*, **2**, 96, 2014.
[37] Shoaib, M., Raja, M. A. Z., Jamshed, W., Nisar, K. S., Khan, I., Farhat, I., *International Communications in Heat and Mass Transfer*, **127**, 105544, 2021.
[38] Ullah, A., Alzahrani, E. O., Shah, Z., Ayaz, M., Islam, S., *Coatings*, **9**, 21, 2018.
[39] Ahmad, A., *Journal of Molecular Liquids*, **219**, 643, 2016.
[40] Raju, C., Sandeep, N., *Acta Astronautica*, **133**, 436, 2017.
[41] De, P., Pal, D., Mondal, H., Bera, U. K., *Journal of Nanofluids*, **6**, 164, 2017.